Phase I trial of Ipatasertib plus Atezolizumab enhances PI3K/AKT pathway immune responses in solid tumors and refractory glioblastoma

Crescens Tiu[1], Wing Yau[1], Diogo Silva[1,2], Nick Waldron[1,2], Malaka Ameratunga[1], Mariana Scaranti[1], Andrea Biondo[1], Liam Welsh[3], Antonia Creak[3], Timothy L. Jones[4,5], Andrew J. Martin[4,5], Lesley Bridges[6], Anna Zachariou[2], Mateus Crespo[2], Ana Ferreira[2], Ruth Riisnaes[2], Bora Gurel[2], Ines Figueiredo[2], Denisa Bogdan[2], Wei Yuan[2], Ricardo Morilla[2], Karen Swales[2], Shaun Decordova[2], Toby Prout[2], Mona Parmar[2], Bindu Baikady[2], Mihaela Rata[2,7], Matthew Blackledge[2], Nina Tunariu[2,7], Phillip Benjamin[3,5], Philip Rich[3,5] Robert Daly[2], Xinjie Hu[8], Christina Yap[8], Igor Vivanco[7], Alec Paschalis[1,2], Adam Sharp[1,2], Udai Banerji[1,2], Anna Minchom[1,2], Johann de Bono[1,2], Juanita Lopez[1,2*]

Running title: Ipatasertib in combination with Atezolizumab for treatment-refractory solid tumors and glioblastoma – ICE-CAP Phase 1 Clinical Trial.

Affiliations:
1 Drug Development Unit at the Royal Marsden NHS Foundation Trust and the Institute of Cancer Research[+], London
2 The Institute of Cancer Research, London[+]
3 Neuro-oncology Unit, Royal Marsden NHS Foundation Trust, London
4 Department of Cellular Pathology, St George's Hospital, London
5 Department of Neurosurgery, Atkinson Morley Wing, St George's Hospital, London
6 Department of Cellular Pathology, St George's Hospital, London
7 MRI Unit, Royal Marsden NHS Foundation Trust, London
8 Clinical Trials and Statistics Unit, The Institute of Cancer Research, London

***corresponding author:** Juanita S. Lopez, Drug Development Unit at the Royal Marsden NHS Foundation Trust and the Institute of Cancer Research, Downs Rd, Sutton SM2 5PT, London. Email: Juanita.Lopez@icr.ac.uk

[+]A member of the imCORE Network

Conflicts of Interest: A.S is an employee of The Institute of Cancer Research (ICR), which holds commercial interests in Abiraterone, PARP inhibition in DNA repair-defective cancers, PI3K/AKT pathway inhibitors, from which he receives no personal income. He has received travel support from Sanofi, Roche-Genentech and Nurix. Speaker honoraria from Astellas Pharma and Merck Sharp&Dohem. A.S has served as an advisor to DE Shaw Research, CHARM Therapeutics, Ellipses Pharma and Droia Ventures.
JDB has served on advisory boards and received honoraria from AbbVie, Acai Therapeutics, Amgen, Amunix, Astellas, Bayer, Bioxcel Therapeutics, Celcuity, Crescendo, Daiichi, Dark Blue Therapeutics, Duke Street Bio, Dunad Therapeutics, Eikon Therapeutics, Endeavor Biomedicines, Genetech/Roche, GSK, Macrogenics, Merck Serono, MetaCurUm, Moma, Morphosys, Myricx, Novartis, Nurix Therapeutics, Nuvation Bio, One-Carbon Therapeutics, Oncternal, Orion, Page Therapeutics, Peptone, Pfizer, Takeda, Tango Therapeutics, Tubulis and Vir Biotechnology. As an employee of the ICR, his institution has also received research funding from AstraZeneca, CellCentric, Crescendo, Daiichi, Immunic Therapeutics, MetaCurUm, Morphosys, Myricx, Nurix Therapeutics, Oncternal, Orion and Sanofi Aventis. The ICR has commercial interests in Abiraterone, PARP inhibition in DNA repair-defective cancers, PI3K/AKT pathway inhibitors, from which he receives no personal income. He is named, without financial interest, on a patent 8,822,438 (Janssen). He has served as CI/PI for multiple industry-sponsored clinical trials and is an NIHR senior investigator.
AM has served in consulting or advisory roles for Merck, Janssen, Pfizer, AstraZeneca, Immutep and MSD; received travel support from Janssen; research grants from Astex, Merck and MSD; honoraria from AstraZeneca, Janssen, Takeda, Seagen and Faron.

AB is an employee of AstraZeneca.
IV has received consulting fees from Aadi Biosciences; research funding from Aadi Biosciences, Roche and Basilea Pharmaceutica; travel support from Aadi Biosciences and Arqule (Merck/MSD).
ACr has served as an advisor to Servier.
KS is an employee of the ICR, which has commercial interests in CYP17, AKT, CHK1, RAF, MPS1, FLT3/Aurora kinase inhibitors, GCN2 activators, molecular glues, and folate-targeted thymidylate synthase inhibitors.
UB has received research grants from Verastem Oncology and Avacta, as well as academic clinical trial grants from Verastem Oncology and Chugai. He has served as a remunerated consultant and on advisory boards for Carrick Therapeutics, Pharmenable, Ellipses Pharmaceuticals, Amalus Therapeutics, Dania Therapeutics and Pegascy. He is an employee of the ICR, which has commercial interests and collaborations involving CYP17, AKT, MPS1 and FLT3/Aurora Kinase inhibitors, molecular glues and folate-receptor-targeted therapies.
JL has received institutional research funding from Roche-Genetech, Basilea, Astex, Taiho, Verastem and Janssen. She has served on advisory boards from Roche-Genetech, Basilea, Servier, GSK and Ellipses Pharma. She is a member of IDMCs for Servier and Ascencion Therapeutics and co-chairs the Tessa Jowell Brain Tumor Novel Therapeutic Accelerator, advising multiple industry partners within the BTR-NTA.

All remaining authors – **CT, WY, DS, NW, MA, MS, LW, TJ, AM, LB, AZ, MC, AF, RR, BG, IF, DB, WY, RM, SD, TP, MP, BB, MR, MB, NT, PB, PR, RD, XH, CY, AP** – declare no conflicts of interest.

ABSTRACT

Purpose: Activation of the phosphatodylinositol-3-kinase/AKT (PI3K/AKT) signalling pathway promotes tumor immune evasion by suppressing effector T-cell infiltration and enhancing regulatory T-cell activity contributing to resistance to immune checkpoint inhibitors. Preclinical studies have demonstrated that inhibition of this pathway can restore anti-tumor immunity and synergize with PD-1/PD-L1 blockade. We explore the synergistic clinical potential of targeting the PI3K/AKT pathway in combination with atezolizumab to overcome immunotherapy resistance in recurrent glioblastoma and advanced solid tumors.

Experimental Design: Phase 1b, investigator-initiated, open-label study (NCT03673787) composed of a proof-of-concept dose escalation Part A of ipatasertib plus atezolizumab in a 3+3 design. Adult patients with treatment refractory advanced cancers were enrolled into Cohort A1 and recurrent glioblastoma onto Cohort A2. Part B enrolled patients into 6 exploratory cohorts. Study aims to evaluate the safety, immune-modulatory effects and preliminary efficacy of the combination of ipatasertib with atezolizumab.

Results: The combination was well tolerated, with no dose-limiting toxicities at the recommended phase 2 dose of ipatasertib 400 mg/daily plus atezolizumab 1200mg every 3 weeks. Pharmacodynamic analysis demonstrated depletion of FOXP3+ regulatory T cells and increased infiltration of CD8+ effector T cells within the tumor microenvironment. Durable exceptional responses were seen in some patients with treatment-refractory or recurrent glioblastoma.

Conclusion: This is the first report in clinical samples showing that ipatasertib efficiently depletes FOXP3+ regulatory T cells and results in increased infiltration of effector CD8+ T cells in the tumor microenvironment. This was associated with preliminary efficacy in a subset of patients with treatment-refractory glioblastoma (GBM).

STATEMENT OF SIGNIFICANCE

This study provides preliminary clinical evidence that blockade of the PI3K/AKT signalling pathway can remodel the immunosuppressive tumor microenvironment and potentially overcome resistance to immune checkpoint inhibitors in malignant recurrent glioblastoma. The combination of the selective AKT inhibitor ipatasertib with the anti-PD-L1 antibody atezolizumab was well tolerated and demonstrated robust immunomodulatory activity, including depletion of FOXP3+ regulatory T cells and increased infiltration of effector CD8+ T cells within the tumor microenvironment, independent of PI3K mutational status or PTEN loss. Durable and exceptional clinical responses were observed in a subset of patients with recurrent, treatment-refractory disease. These results highlight PI3K/AKT pathway inhibition as a mechanistically rational and clinically feasible strategy warranting broader evaluation in this cancer of unmet need.

INTRODUCTION

The phosphoinositide 3-kinase (PI3K)-AKT signalling pathway regulates a wide range of cellular processes, including growth and survival (1, 2). Hyperactivation of this pathway is a critical driver of tumorigenesis, with phosphatase and tensin homolog (PTEN), being one of the most common targets of mutation/deletion in human tumors. Other mechanisms of PI3K-AKT pathway deregulation include *PI3KCA* mutations, *AKT* amplification and mutations, overexpression (transcriptional upregulation) and activation downstream of the AKT pathway (3). Deregulation of this pathway is a frequent hallmark of tumor resistance to chemotherapy, targeted therapies, and more recently, immunotherapy(4-6).

The PI3K-AKT pathway has been implicated in the regulation of both innate and adaptive immunity and plays crucial roles in immune cell maturation, differentiation, recruitment, and survival(5). AKT has also been shown to control regulatory T cells (Treg) homeostasis through inhibitory phosphorylation of FOXO1, which in turn promotes immune tolerance by restraining immune effector cells (7-11).

Despite the successes of immune checkpoint inhibitors (ICIs) targeting the PD-1/PD-L1 and CTLA-4 immune checkpoints, many cancers do not respond or respond incompletely to immunotherapy(12, 13). While a myriad of mechanisms can underlie ICI treatment failure, the profound immunosuppressive tumor microenvironment rich in inhibitory Tregs has been associated with hyperactive PI3K-AKT signalling. Thus, ICI resistance may be reversible by blockade of this pathway(14-18). Preclinical studies in multiple solid tumor models have shown increasing evidence that targeting the PI3K-AKT pathway, and AKT in particular, can reduce the production of immunosuppressive cytokines such as IL10 and TGFβ(19-21). Reduction of IL10 and TGFβ restricts the proliferation and penetration of immunosuppressive Tregs and inhibits M2 macrophage polarization, boosting the anti-tumor effects of immune checkpoint blockade (22, 23). Co-inhibition of the PI3K pathway has improved the efficacy of anti-PD-1 and anti-CTLA-4 antibodies in PTEN-driven murine models of melanoma (24) as well as syngeneic murine models of breast and lung cancer (25, 26). Additionally, the pharmacological inhibition of the PI3K-AKT pathway in *in vitro* patient cell assays showed inhibition and reduction in Treg populations and enhancement of the $CD8^+$ memory T-derived tissue (27). Given that many of the immunosuppressive effects of PI3K activation seem to be mediated by AKT and because AKT inhibitors appear to be generally safer compared to PI3K inhibitors, combination strategies using AKT inhibitors are likely preferable (28).

We conducted an open-label proof-of-concept Phase 1b clinical trial to interrogate the effect of PI3K-AKT blockade on the immune system, and its synergy with ICIs for effective cancer immunotherapy. Mandatory serial blood and tumor sampling allowed for comprehensive translational analyses.

We report, for the first time, the safety and tolerability of the combination ipatasertib, a potent AKT inhibitor, with the anti-PD-L1 ICI, atezolizumab, and describe the pharmacodynamic effects of PI3K-AKT blockade on the immune system and the tumor microenvironment (TME). We report preliminary efficacy in a subset of patients with treatment-refractory glioblastoma (GBM).

METHODS

The study was conducted in accordance with the ethical principles derived from international guidelines including the Declaration of Helsinki. The study protocol was approved by the MHRA and ethics committee and all patients provided written informed consent.

Study design

This was an open-label, single centre phase 1 study in patients with treatment refractory advanced solid tumors and glioblastoma (NCT03673787). The trial commenced in August 2018 and contained two parts: 1) Part A: proof-of-concept dose exploration of the combination of oral ipatasertib given continuously with three weekly doses of atezolizumab 1200mg intravenously. Dose escalation decisions for the solid tumor patients in Cohort A1 were guided by a 3+3 design, while patients with GBM in Cohort A2 were enrolled at the dose level cleared in Cohort A1. 2) Part B enrolled patients into 6 exploratory cohorts (**Figure 1A)**. Data presented here are from Part A and GBM exploratory cohort B3 as of September 2024.

The primary objectives of the dose exploration part were to evaluate the safety and tolerability of the combination of ipatasertib and atezolizumab and to determine the maximum tolerated dose (MTD) and the recommended dose for Phase 2 (RP2D). The secondary objectives were to characterize the pharmacodynamic effects of PI3K-AKT blockade by single agent ipatasertib, and the combination with atezolizumab, on immune parameters in blood and tumor. Tertiary objectives were to obtain a preliminary assessment of anti-tumor efficacy in patients with tumors resistant to ICIs.

Patient Selection

Adult patients aged ≥18 years were included if they had histologically or cytologically confirmed advanced solid cancer refractory to standard therapy. Patients enrolled onto Cohort A1 needed to have biopsiable disease, while GBM patients enrolled onto Part A2 needed to have disease potentially suitable for re-resection/surgical biopsy. Key inclusion criteria also required that patients had an Eastern Cooperative Oncology Group (ECOG) functional status 0 or 1 and had adequate organ function. Key exclusion criteria were autoimmune disorders requiring immunosuppression. Full eligibility criteria are further detailed in the Supplementary Methods.

Treatment

Ipatasertib was administered orally daily in 21-day cycles, and atezolizumab was administered as an intravenous infusion every 21-days. Dose escalation commenced at the minimum anticipated biological effect level–defined starting dose of ipatasertib (200mg daily continuously) and progressed up according to the dosing schema to 400mg daily continuously.

Patients in Part A were given a run-in period with ipatasertib monotherapy of 14-21 days (**Figure 1A**) to allow for collection of serial blood and tumor samples for pharmacodynamic analyses.

Analysis Populations

All safety endpoints were summarized using the Safety Population, which comprised of all patients who had received at least one dose of ipatasertib or one dose of atezolizumab and who had at least one post-dosing safety evaluation.

All baseline characteristics and demographic are reported per the safety evaluable population; efficacy data as per the efficacy evaluable population and pharmacodynamic data analysed using the tissue available population (**Supp. Tables 1 and 2**). For Part A, all patients who had completed the Cycle 1 DLT period (i.e. 35 days) and received at least 75% of the specified dose of ipatasertib (i.e. at least 27 doses out of the planned 35) and received C1D1 dose of atezolizumab were considered evaluable for purposes of dose escalation decisions. For Part B dose expansion, the population comprised of all patients who received at least one partial or complete cycle of ipatasertib and atezolizumab combination therapy.

Efficacy Analysis

Efficacy analysis included assessment of objective response (OR), duration of response (DOR), PFS and OS from start of combination treatment. OR was assessed as per immune-modified Response Evaluation Criteria in Solid Tumors (iRECIST) criteria or immunotherapy Response Assessment in Neuro-Oncology (iRANO) criteria(31, 32). Radiographic tumor burden assessments were assessed by the investigator and could include CT, MRI, and bone scans. Assessments were performed at baseline, at week 9 and every subsequent 9 weeks until study discontinuation. Details of imaging acquisition are detailed in the supplementary data.

Statistical Considerations

The sample size in the dose-exploration proof-of-concept Part A was based on practical consideration and was consistent with conventional oncology studies with the objective to estimate the MTD and obtain proof-of-mechanism. Two dose levels were explored starting at the minimum biologically active dose and escalated per the 3+3 design following review by the Safety Review Committee (SRC).

Translational and pharmacodynamic endpoints

Peripheral blood lymphocyte profiling

In Part A, to assess the effect of single agent AKT inhibition, whole peripheral blood was collected at baseline (C1D-14 for Cohort A1 or -21 for Cohort A2), and after 14-21 days of continuous ipatasertib monotherapy (pre-infusion on C1D1, or 48 hours prior to surgery for Cohort A2). Subsequent samples to assess the effect of the combination of AKT inhibition and atezolizumab were collected on D1 of each cycle until treatment discontinuation. Samples were stained with monoclonal antibodies against the following cell-surface markers: CD3, CD4, CD8, CD5, CD56, CD19, CD20 and CD45. Stained cells were acquired and analysed on a Cytoflex LX (Beckman Coulter) cytometer using Kaluza version 2.1 software (RRID:SCR_016182).

Serum cytokine profiling

Blood samples for cytokine profiling were collected in 5mL BD SST II Plus Vacutainer tubes at the same timepoints listed above. Cytokine concentrations (pg/mL) were measured by the multiplex MesoScale Discovery V-Plex Plus Human Pro-Inflammatory Panel 1 Kit (K15049G) customised by MSD to detect only for IFNg , IL-1b, IL-2, IL-6, IL-8, IL-10, and TNF-a. Log2 fold change of cytokine concentrations from baseline (C1D-14 or -21) to post-ipatasertib (C1D1) were calculated for each patient. Concentrations below the lower limit of quantification were included in the calculations. Concentrations below the assay lower limit of detection

(LLOD) were set as the LLOD value. Patients 101-051 and 101-057 were excluded as post-ipatasertib samples were not available. TNF-a concentrations for patient 101-038 were excluded due to quality control failure. Comparisons were performed using paired t-test, with p-value of 0.05 being statistically significant.

Tumor analysis

Mandatory paired tumor biopsies were collected from all patients enrolled onto Cohort A1 at baseline, and following 14 days of continuous ipatasertib monotherapy, with additional optional biopsies collected after the first cycle of combination ipatasertib and atezolizumab. At each timepoint, two needle core biopsies (size 14-16 gauge) under ultrasound guidance. Three 3-µm sections of tumor were stained with haematoxylin and eosin (H&E), and presence of tumor was confirmed by a pathologist (author BG). Paired samples were analysed by multi-IF (mIF) for tumor infiltrating lymphocytes (TILs). An FFPE block was submitted to HistoGeneX (Kluisbergen, Belgium) for immunophenotyping, PDL-1 assessment, and nucleic acid extraction. RNA and whole exome sequencing was performed by Q Squared Solutions (Morrisville, NC, USA). GBM patients on Cohorts A2 and B3 provided archival FFPE samples for similar analyses, as well as IHC for PTEN status. Patients with potentially resectable disease and who had agreed to proceed to surgery had tumor cores collected for analyses.

5-plex immunofluorescence (CD3, CD4, CD8, FOXP3 and PanCK) for Cohort A1

TILs were determined by mIF for T cell subpopulations as previously described (33). mIF staining was performed on 3µm FFPE tissue sections using an automated staining platform (BOND RX, Leica Microsystems). Antigen retrieval was achieved using BOND Epitope Retrieval Solution 2 (#AR9640, Leica Biosystems). Endogenous peroxidase was inactivated in 3% H_2O_2. Tissue sections were incubated with antibodies against CD4 (#ab133616, clone EPR6855, Abcam) and CD8 (#M7103, clone C8/144B, Dako, Agilent Technologies; RRID:SCR_013575)), and detected with AlexaFluor 555-conjugated IgG (H+L) goat anti-rabbit (#A21429, Invitrogen; RRID:AB_2535850) and AlexaFluor 488-conjugated IgG (H+L) goat anti-mouse (#A-11029, Invitrogen; RRID:AB_2534088) secondary antibodies, respectively. Endogenous biotin was blocked with Avidin/Biotin blocking kit according to the manufacturer's protocol (#ab64212, Abcam). Tissue sections were incubated with antibodies against FOXP3 conjugated to biotin (#13-4777-82, clone 236A/E7, eBioscience, ThermoFisher; RRID:AB_466655) and pan-cytokeratin (PanCK) conjugated to AlexaFluor 647 (#4528S, clone C11, Cell Signaling Technology; RRID:AB_836890), followed by streptavidin peroxidase (HRP) (#K5001, Dako, Agilent Technologies) and TSA Coumarin detection system (#NEL703001KT, Akoya Biosciences). Nuclei were counterstained with DRAQ 7 (#DR71000, Biostatus) and tissue sections mounted with ProLong Gold antifade reagent (#P36930, Molecular Probes).
Slides were scanned using the Vectra Automated Multispectral Imaging System (Akoya Biosciences) and analyzed using inForm v2.2.1 (Akoya Biosciences). Tissue and nuclear cell segmentation were performed using previously described methods (34). TIL phenotype determination was based on staining for CD8, CD4, and FOXP3 and were separated into bins as follows: CD8+, CD4+FOXP3+, and CD4+FOXP3- T cells.

4-plex immunofluorescence (CD3, CD4, CD8 and FOXP3) for Cohorts A2 and B3

4-plex OPAL-based sequential immunofluorescence staining was performed on the Bond RX automated staining platform (Leica Biosystems). Three 3-µmFFPE tissue sections underwent heat-induced epitope retrieval with BOND epitope retrieval solution 2 (pH 9.0) (#AR9640,

Leica Biosystems) for 20 minutes, followed by endogenous peroxidase blocking (Novocastra™ Peroxidase Block, #RE7157, Leica Biosystems) for 10 minutes. Non-specific antibody binding was blocked using Opal Antibody Diluent/Block (ARD1001EA, Akoya Biosciences) for 10 minutes. Primary antibodies against CD3 (#A0452, Rabbit Polyclonal Antibody, Dako, RRID:AB_2335677), CD4 (#ab133616, clone EPR6855, Abcam, RRID:AB_2750883), CD8 (#M7103, clone C8/144B, Dako, Agilent Technologies, RRID:AB_2075537) and FOXP3 (#14-4777-82, clone 236A/E7, eBioscience, ThermoFisher, RRID:AB_467556) were sequentially incubated for 30 min followed by detection with Novolink Max Polymer Detection System (RE7280-K, Leica Biosystems). mIF signals for CD8, CD4, FOXP3 and CD3 were visualised using OPAL 520, OPAL 570, OPAL 620 and OPAL 690 (NEL871001KT, Opal 6-Plex Detection Kit, Akoya Biosciences), respectively, and counterstained with spectral DAPI (FP1490, Akoya Biosciences). Automated imaging was performed on the PhenoCycler™- Fusion system (Akoya Biosciences, Menlo Park, CA) using the instrument controller software v1.0.7 (Akoya Biosciences, Menlo Park, CA).

mIF images were reviewed by a pathologist (author BG). Analysis was performed using HALO image analysis software (Indica Labs, New Mexico, USA). Cell detection was based on nuclear DAPI counterstain, with nuclear diameter thresholds of 8 µm (minimum) and 25 µm (maximum). Nuclear segmentation parameters were optimised to detect individual nuclei while minimising over-segmentation of clustered cells. Cell phenotyping used intensity thresholds for each fluorescence channel (OPAL 520, 570, 620 and 690), which were set by comparing signal intensities in positive and negative control tissue sections stained on the same slides. These thresholds remained constant across all analysed images. T lymphocyte populations were classified using Boolean logic based on marker combinations: CD3+CD4+CD8-FOXP3- (T helper cells), CD3+CD4-CD8+FOXP3- (cytotoxic T cells), and CD3+CD4+FOXP3+ (regulatory T cells). The accuracy of cell classification was verified through manual review of representative image fields.

4-plex immunofluorescence (macrophages) for Cohorts A2 and B3

4-plex OPAL-based sequential IF staining was carried out on the Bond RX automated staining platform (Leica Biosystems). FFPE tissue sections of 3 µm underwent heat-induced epitope retrieval with epitope retrieval solution 1 (pH 6.0; No. AR9961, ER1, Leica Biosystems) followed by endogenous peroxidase blocking (Novocastra Peroxidase Block, No. RE7157, Leica Biosystems) for 10 min. Nonspecific antibody binding was blocked using OPAL antibody diluent/block (ARD1001EA, Akoya Biosciences) for 10 min. Primary antibodies against CD206/MRC1 (CST, #91992, 1:250; RRID:AB_2800175), #CD68 (Dako #M0876, 1:200; RRID:AB_2074844), CD163 (Abcam, #ab182422, 1:200; RRID:AB_2753196) were sequentially incubated for 30 min followed by detection with the Novolink Max Polymer Detection System (RE7280-K, Leica Biosystems). IF signals for CD206, CD68 and CD163 were visualized using OPAL 520 (NEL820001KT, Akoya Biosciences), OPAL 570 (NEL820001KT, Akoya Biosciences) and OPAL 650 (FP1496001KT, Akoya Biosciences), respectively, and counterstained with spectral DAPI. Slides were scanned using the VS200 Research Slide Scanner (Olympus).
Exploratory statistical analysis of immune cell counts from multiplex IF and flow cytometry were performed using two-tailed unpaired t-test was performed using Graphpad Prism (RRID:SCR_002798).

PD-L1 and immune phenotyping

FFPE samples were submitted to HistoGeneX for analysis according to their standard operating procedures. This included H&E assessment, PD-L1 SP263 IHC and PanCK/CD8 IHC. Cytoplasmic staining was not included in the scoring (TE-IQ-16 method on FO-390,

HistoGeneX). The PanCK-CD8 IHC slides were evaluated for CD8 using the universal immune cell marker scoring algorithm (TE-IQ-40 and FO-526, HistoGeneX). The output of this analysis was the relative surface area (%) of the tumor with a CD8+ immune cell density that belongs to one of the 8 density bins, and for each of the 8 density bins (8 data fields per IHC slide). The density bins were linked to marker-specific (CD8) reference images that were used by the pathologist. The immune phenotype was scored as 'desert', 'inflamed', or 'excluded' (two types: invasive margin or intratumoral). PanCK was automatically detected to generate an epithelial carcinoma mask in the annotated tumor region. The relative surface area of CD8+ TILs was then measured in both stromal and epithelial (carcinoma cell nests) compartments using image analysis applications.

RNA and whole exome sequencing

RNA expression profiling was performed by Q Squared Solutions (Morrisvile, NC, USA) using Illumina TruSeq RNA Access chemistry on the Illumina sequencing platform with a 50bp paired end strategy and target of 40 million average reads across all samples. Genomic DNA was analysed using Agilent SureSelect 60 Mb Kit; Exome Seq SureSelect v6 followed by Sequencing on the Illumina platform with a 63M reads 100bp paired-end strategy.

PTEN IHC

PTEN protein expression was determined by IHC on 4-µm-thick FFPE as previously described (34-36). PTEN immunoreactivity was investigated using rabbit monoclonal anti-PTEN antibody (#9559, clone 138G6 Cell Signaling Technology, Danvers, MA, USA; RRID: AB_390810) and a Vectastain Elite ABC kit (Vector Laboratories, Burlingame, CA, USA). The intensity of nuclear and cytoplasmic staining was semiquantitatively assessed using the H-score formula as previously defined (35). Based on a previous PI3K inhibitor trial on solid tumors, loss of PTEN function was defined as H-score <30, with a maximum of 30% of cells at a 1+ staining intensity(26). PTEN-positive controls included normal prostate tissue and 22RV1 xenograft tissue, and PTEN-loss controls included PC3 (PTEN-null prostate cancer cell line) xenografts. Endothelial cells and stroma were used as internal positive controls for PTEN. All IHC sections were evaluated by a pathologist (author BG) blinded to the patients' clinical characteristics and outcome data.

RNA transcriptomics analysis

Paired-end transcriptome reads were aligned to the human reference genome (GRCh38/hg38) using the STAR splice-aware aligner (v2.7.7a - RRID:SCR_004463). Raw gene expression counts were calculated with the Subread package (v2.0.1) and used for differential expression analysis with the DESeq2 package (v1.32.0 - RRID:SCR_000154). Normalized gene expression was reported as calculated internally by DESeq2 using normalization to the geometric mean expression across replicates. Pathway enrichment scores were calculated with the GSVA package (v1.52.3) using the zscoreParam method with default parameters. The results were obtained using the H collection of Hallmark gene sets (MSigDB v7.0) and cell state signature from Thommen, D.S et al. and Hanjie Li et al. (40,41) (**Supp. Table 5**). Kaplan-Meier survival curves were generated using the OS clinical data. P-values reported were calculated using the log-rank test. Patients were stratified into low [Quartile (Q)1], medium (Q2-Q3) and high (Q4) groups by the median value of the predictor variable across the cohort.

Data availability: The data that support the findings of this study are not publicly available due to patient privacy requirements but are available from the corresponding author, upon reasonable request.

RESULTS

A total of 47 patients with advanced solid tumors or relapsed GBM were enrolled to the trial between August 2018 and September 2024 (**Figure 1**). Patient demographics are described in **Table 1**. Patients in the solid tumor Cohort A1 were heavily pre-treated, having received a median of 5 (range 1-11) prior lines of therapy for advanced disease. All patients with relapsed GBM had at least one prior line of treatment (range 1-4). A summary of mutation distribution and immune phenotype is provided in **Supp Tables 1 and 2**. This report describes results from the proof-of-concept Part A and the exploratory GBM cohort B3.

Dose exploration

Part A enrolled 32 patients across two planned dose levels. Accrual of GBM patients in Cohort A2 ran in parallel to the solid tumor Cohort A1, with patients enrolled at the highest dose level deemed tolerable for patients with solid tumors. As enrolment to the GBM cohort commenced prior to publication of the 2021 WHO Classification of Tumor of the Central Nervous System, this cohort also included 2 patients with Astrocytoma IDH mutant WHO Grade 4. Although we utilised a 3+3 model for dose escalation in cohort A1 (only), patient recruitment continued at the Recommended Phase 2 Dose (RP2D) to enable completion of the translational proof-of-concept studies from 12 evaluable patients. Similarly, patient recruitment continued in cohort A2 to ensure acquisition of post-dosing resection tissue from 3 patients **(Figure 1A)**.

In Cohort A1, there was one dose-limiting toxicity (DLT) of Grade (G) 3 raised ALT at dose level 1 (n=9); no DLTs were seen at dose level 2 (n=7). There were no DLTs seen in patients with relapsed GBM across the two dose levels tested in Cohort A2. The RP2D of the combination was established as oral ipatasertib 400mg daily continuously plus intravenous atezolizumab 1200mg three-weekly.

Safety

A total of 43 patients were included in the safety evaluable population. Treatment-emergent adverse events (TEAE) were reported in 43 patients, with 35 (84%) patients reporting at least one treatment-related adverse event (TRAE), defined as any TEAE deemed by the investigator to have a reasonable possibility of being caused by ipatasertib or atezolizumab; (**Table 2 and Figure 2**).

In Cohort A1 (n=18), the most common TRAEs were G1-2 diarrhoea (61%), rash (50%), nausea (39%), fatigue (39%), and asymptomatic transaminitis (39%) which were easily reversible. G3 TRAEs included transient and rapidly reversible rash and asymptomatic transaminitis **(Figure 2A).** Hyperglycaemia was mild (G1 and G2 in 6% of patients) and did not require any dose interruptions or modifications. The severity of cutaneous rashes was most pronounced in Cycle 1, with subsequent habituation permitting continuation of dosing. There were no treatment-related fatalities on study. The only G5 adverse event was a chest infection in a patient with progressive disease-related lymphangitis proven on imaging.

The safety profiles in the GBM cohorts (A2 and B3) were consistent with Cohort A1, with the most common TRAEs being G1-G2, including diarrhoea (64%), rash (28%), fatigue (20%) and asymptomatic transaminitis (20%). G3 TRAEs were only seen in 8%, with rash and asymptomatic transaminitis being the most common **(Figure 2B).** There were no treatment-related fatalities in the GBM cohorts.

Across all cohorts, TRAEs led to dose interruption (missed doses) in 16 patients (37.2%) and dose reduction in 5 patients (11.6%). The most common reasons for dose interruption and

reductions were rash (32%); diarrhoea (16%); transaminitis (16%) and fatigue (16%). No patient discontinued dosing due to TRAEs.

Efficacy

Solid tumor Cohort A1. Two patients (pts) with metastatic treatment refractory hormone receptor positive breast cancer had confirmed partial responses (PR) in the cohort A1 efficacy evaluable population (n=16). Seven pts (43.8%) had radiological stable disease (SD), with four achieving SD >16 weeks (25%). Overall response rate (ORR) was 12.5% [95% CI 2.2 – 39.6] and clinical benefit rate (CBR) was 37.5% (95% CI 16.3-64.1) (i.e. combined PR and SD >16 weeks*).* The median progression free survival (PFS) from start of combination therapy was 2.1 months [95% CI 0.6 months – not reached (NR)], with a 3-month PFS rate of 33.3 (95% CI 15.9-70.0) and 6-month PFS rate of 16.7% (95%CI 4.9-57.0). All five breast cancer patients who benefitted from the combination treatment (i.e. PR or SD >16 weeks) had low T-cell counts at baseline biopsies **(Supp. Table 1)**. Three of the breast cancer patients benefitting from treatment (1 ER-HER2+ and 2 ER+HER2-) did not have any detectable aberration in the PI3K pathway **(Supp. Table 1)**.

GBM Cohorts A2 and B3. Twenty efficacy evaluable patients with recurrent GBM were enrolled across Cohorts A2 and B3, of which 16 patients (80%) had PTEN loss by IHC (H-score <30) indicative of biallelic loss of function. (**Supp. Table 2**).
CBR in the overall GBM population was 30% (95% CI 12.8 – 54.3), 25.0% (95% CI 1.3 – 78.1) for PTEN intact and 31.3% (95% CI 12.2 – 58.5) for patients with PTEN loss (**Figure 3C**, **Supp. Table 2**).

Additional analysis of overall survival (OS) from trial entry in this heavily pre-treated relapsed GBM population showed a median OS of 8.81 months (95% CI 5.52 – NR). Median OS was 8.55 months (95% CI 4.57 – NR) for patients with PTEN loss (n=16), and 8.81 months (95% CI 6.84 – NR) for those with PTEN intact tumors, respectively (**Figure 3D**). The 12-month OS rate (OS12) was 33.85% (95% CI 17.96 – 63.8) comparing favourably with the OS12 rate observed in contemporary recurrent GBM trials. Here we describe 3 cases of GBM patients who had prolonged responses.

A 58-year-old male (ICE101019) with recurrent glioblastoma (PTEN loss) progressed to surgery following 5 cycles of ipatasertib and atezolizumab. Magnetic resonance imaging (MRI) had shown increase in contrast-enhancing disease, albeit with a significant rise in Apparent Diffusion Coefficient (ADC), suggestive of pseudoprogression **(Figure 3A).** Histopathological analyses of the resection sample showed maintained high levels of CD8+ lymphocyte infiltration, increase in CD4+FOXP3- Th cells, with no residual evidence of tumor (pathological CR) **(Figure 3A, 4G)**. The patient resumed treatment on trial with PFS of 23 months.

A 64-year-old female (ICE101106, PTEN loss) with multiple relapsed GBM that had progressed through radical chemo-radiotherapy and second line lomustine had a confirmed PR (-90% per iRANO) maintained for more than 12 months **(Figure 3B).**

One additional patient, a 55-year-old male (ICE101045, CH, PTEN loss), discontinued study treatment due to clinical symptoms at 6 weeks but remained clinically stable off trial for over 12 months.

Regulatory T cell modulation by AKT inhibition

Ipatasertib monotherapy at the dose levels used in this study has already been shown to inhibit multiple downstream PI3K-AKT targets in paired blood and tumor samples from patients with advanced cancer, confirming target modulation of this pathway (29). We show, for the first

time, that ipatasertib induces significant depletion of T_{regs} in both solid tumors and GBM, resulting in increased infiltration of CD8+ effector T cells in responding patients.

To quantify changes in T cell populations in the TME, tumor biopsies were analysed using multiplex immunofluorescence (mIF) staining for T cell markers CD4, CD8, FOXP3. After two weeks of ipatasertib, at both dose levels, a reduction in CD4+ FOXP3+ Tregs in the TME was seen in Cohort A1 (8 breast cancer, 1 cervical cancer), regardless of PI3K pathway mutation status (**Figure 4A-B**). There were no significant changes in PD-L1 expression at these time points (**Supp. Figure 1).**

Overall, five breast cancer patients and one cervical cancer patient had evaluable serial biopsies at three timepoints: baseline, post-ipatasertib (C1D1) and following the combination of ipatasertib and atezolizumab (C2D1). Two of the PIK3CA wildtype breast cancer patients, (1 ER+ HER2-, 1 ER+ HER2+), had marked increase in intratumoral CD8+ T cell infiltration by Cycle 2, effectively switching from a *desert* phenotype to an *inflamed* phenotype, with clinical benefit maintained for more than 4 cycles (**Figure 4B-C**). These findings were consistent with FACS analysis of blood samples from the entire solid tumor cohort which showed increase in CD8+ lymphocytes in responders after ipatasertib alone and post-combination treatment (**Supp. Figure 3**).

Two GBM patients (1 PTEN intact, 1 PTEN loss by IHC) in Cohort A2 had planned re-resection of tumor after 2 weeks of ipatasertib monotherapy for pharmacodynamic analyses **(Figure 4D)**. Both had reductions in CD4+FOXP3- helper T (Th) cells and CD4+FOXP3+ Treg cells in the TME (**Figure 4E**). At this early timepoint following ipatasertib monotherapy, one patient (ICE101016, PTEN intact) with a marked increase in CD8+ effector T cells, achieved SD **(Figure 4E-G);** while the other patient (ICE101038, PTEN loss), who only minimally incremented CD8+ cells, had PD (**Figure 4E**). The exceptional responder (ICE101019, PTEN loss) who progressed to surgery after 5 cycles of ipatasertib with atezolizumab, had high levels of CD8+ effector T cells at baseline which remained elevated in the resected tumor. **(Figure 4H)**. There was also significant increase in CD4+FOXP3- Th cells, with no evidence of residual tumor **(Figure 3A, 4I).** In all three patients, there was an increase in Th/Treg ratio post treatment, with the greatest change seen in the exceptional responder's surgical sample taken after ipatasertib-atezolizumab combination. Between both patients who had samples taken after ipatasertib monotherapy, the patient who achieved SD had a greater Th/Treg shift compared to the patient who had PD **(Figure 4J)**. These data suggest that ipatasertib can shift CD4+ T cells towards a Th phenotype, which may correlate with response.

We investigated the archival tumor samples from all GBM patients to identify biomarkers associated with treatment effect and clinical outcomes. We explored the impact of PTEN loss on the TME by analysing the major immune subsets (CD8+ effector T cells, CD4+FOXP3+ Tregs and CD4+FOXP3- Th cells) in archival samples. The abundance of these immune cells was largely similar between the PTEN intact and PTEN loss GBM tumors **(Supp. Figure 2),** consistent with our clinical observation that benefit was seen in both patient subgroups (**Figure 3C).**

CD8+ effector T cells at baseline were significantly more abundant in archival tumor samples of patients with clinical benefit compared to non-responders **(Figure 5A)**. Transcriptomic analysis showed that patients with clinical benefit had higher CD8A expression at baseline **(Figure 5B)**. Patients were stratified into CD8A mRNA low, medium and high expression. High CD8A expression correlated with better OS (**Figure 5C**).

We then performed unsupervised clustering analysis based on activities from hallmark gene sets and correlated this with CD8A expression (**Figure 5D**). All responders were in the CD8A high (4/5) and medium groups (4/10), compared to none (0/5) in the low CD8A group. Notably, 4/5 patients who had high CD8A signature also displayed exhaustion phenotypes, but then

derived clinical benefit, suggesting that combination treatment was able to overcome the T cell exhaustion state. In the CD8A medium group, 75% (3/4) responders tended to have upregulated PI3K signalling and several inflammatory response pathways, compared to only 30% (3/10) of non-responders. This suggests that CD8A medium tumors might rely more on PI3K activation in concert with other inflammatory pathways to achieve response.

Additional mIF analysis of tumor-associated macrophages (TAMs) was performed in three available pairs of window-of-opportunity (WOO) GBM samples (**Supp. Figure 4**). In patient ICE101016, who achieved SD, post-ipatasertib samples showed a reduction in overall TAM density, including M2-like immunosuppressive subsets (**Supp. Figure 4B-C**). This observation, together with the previously reported reduction in Tregs in the same patient (**Figure 4E**), is consistent with published reports suggesting that PI3K–AKT pathway inhibition may be associated with modulation of the immunosuppressive tumor microenvironment, including effects on Treg infiltration and M2 macrophage polarization. As this analysis was exploratory and not pre-specified among translational endpoints, these findings require further validation.

Lastly, we compared paired serum cytokine levels taken before and after the ipatasertib run-in period. There were no significant changes in Cohort A1, with no differences when comparing between response groups or PIK3CA/AKT mutation status. In the GBM Cohort A2, there was suppression of IL-6 in the PTEN intact group compared to PTEN loss, although this difference was not observed between responders and non-responder groups (**Supp. Figure 5**).

DISCUSSION

There remains an unmet need for effective strategies to overcome resistance to immunotherapy. Numerous studies have demonstrated that activation of the PI3K-AKT pathway in tumors promotes an immunosuppressive TME through multiple mechanisms, and resistance to ICI(29). Inhibiting this pathway in combination with immunotherapy may be a strategy to improve outcomes. We present, for the first time in patients, the immune-modulatory effects of PI3K-AKT signalling pathway blockade on the TME and preliminary efficacy of the combination of AKT inhibitor and ICI in relapsed GBM. Our clinical trial results and translational data provide further insights into targeting the PI3K-AKT pathway with brain penetrant potent inhibitors as a promising strategy to overcome resistance to immunotherapy in GBM.

To date, most clinical studies utilising inhibitors of the PI3K-AKT blockade have been strategically focused on combinations with endocrine therapies or chemotherapy in patient populations selected for aberrations in this pathway (e.g. PI3K mutations in breast cancer, or PTEN loss in prostate cancer). A Phase 1 combination study of the PI*3Kβ* specific inhibitor GSK2636771 with pembrolizumab (NCT01458067) in patients with PTEN loss advanced cancer has recently closed. This study reported significant toxicity, with the combination RP2D using a considerably lower dose than the monotherapy dose(30). Our study shows that overall, the combination of the ATP-competitive allosteric inhibitor of AKT, ipatasertib with atezolizumab, was well tolerated with a safety profile that was monitorable, manageable and reversible at the RP2D. We also demonstrate, across a broad range of solid tumors and GBM, that blockade of the PI3K-AKT pathway with ipatasertib at 400mg oral daily is associated with depletion of immunosuppressive regulatory T cells within the TME, which does not seem to be correlated with tumor somatic PI3K mutational or PTEN expression status. Considerable increases in CD8+ T cells were observed in tumor of two breast cancer patients and 1 GBM patient who benefitted from the combination treatment. Notably, although ipatasertib was not designed as a brain penetrant molecule, given the significant leakiness of the blood-brain-barrier in GBM, we were able to demonstrate pharmacodynamic modulation of the immune

microenvironment mirroring that seen in the solid tumor patients, alongside preliminary clinical benefit.

Luminal (ER+) breast cancers are known to be immunologically “cold” tumors and poorly respond to single agent immune checkpoint inhibitors. In our study, clinical benefit was observed in 50% (3/6) of luminal breast cancer patients despite all patients having PDL-negative and immune desert/excluded tumors. Notably, we observed immune alterations including Treg depletion during ipatasertib monotherapy, followed by CD8+ T cell increase upon addition of atezolizumab. Together, these findings are consistent with a model in which AKT inhibition contributes to immune remodelling in otherwise immunologically cold luminal breast cancers, potentially increasing susceptibility to ICI-based therapy.

Although direct pharmacodynamic confirmation of AKT pathway inhibition in tumor biopsies was not feasible due to limited tissue availability and prioritization of immune profiling, the association between AKT inhibition and the observed immune effects is supported by multiple lines of evidence. These include the well-established on-target activity of the compound at the administered dose(29), extensive preclinical and clinical data demonstrating AKT-dependent regulation of Treg survival and function (7-11), and prior reports showing inhibition of T regs following AKT pathway targeting(22). Finally, despite the immune changes noted after the ipatasertib run-in period, we acknowledge that definitive attribution of immune remodeling as a result of AKT inhibition alone, immune checkpoint blockade, or interactions between the two agents will require larger trials incorporating an atezolizumab-alone comparator arm. While ICI trials have been disappointing for treatment of GBM, it is noteworthy that a subset of our patients did respond well. There were some patients with prolonged clinical benefit and disease control, including patients with multiple relapsed GBM, a disease that is known to be resistant to immunotherapy. Analyses are only descriptive, with relatively low event numbers. Further expansion of the combination in relapsed GBM could not be pursued due to the pharmaceutical company’s strategic decision to cease development of ipatasertib in new disease areas. Future work will now focus on reverse translation into clinically relevant syngeneic models of GBM to further evaluate the potential benefit of targeting the PI3K-AKT pathway with more potent brain penetrant inhibitors for combination strategies with immunotherapy.

REFERENCES

1. Fruman DA, Chiu H, Hopkins BD, Bagrodia S, Cantley LC, Abraham RT. The PI3K Pathway in Human Disease. Cell. 2017;170(4):605–35.
2. Fruman DA, Rommel C. PI3K and cancer: lessons, challenges and opportunities. Nat Rev Drug Discov. 2014;13(2):140–56.
3. Bailey MH, Tokheim C, Porta-Pardo E, Sengupta S, Bertrand D, Weerasinghe A, et al. Comprehensive Characterization of Cancer Driver Genes and Mutations. Cell. 2018;173(2):371–85 e18.
4. LoRusso PM. Inhibition of the PI3K/AKT/mTOR Pathway in Solid Tumors. J Clin Oncol. 2016;34(31):3803–15.
5. Okkenhaug K, Graupera M, Vanhaesebroeck B. Targeting PI3K in Cancer: Impact on Tumor Cells, Their Protective Stroma, Angiogenesis, and Immunotherapy. Cancer Discov. 2016;6(10):1090–105.
6. Engelman JA. Targeting PI3K signalling in cancer: opportunities, challenges and limitations. Nat Rev Cancer. 2009;9(8):550–62.
7. Ouyang W, Liao W, Luo CT, Yin N, Huse M, Kim MV, et al. Novel Foxo1-dependent transcriptional programs control T(reg) cell function. Nature. 2012;491(7425):554–9.
8. Luo CT, Liao W, Dadi S, Toure A, Li MO. Graded Foxo1 activity in Treg cells differentiates tumour immunity from spontaneous autoimmunity. Nature. 2016;529(7587):532–6.
9. Granville CA, Memmott RM, Balogh A, Mariotti J, Kawabata S, Han W, et al. A central role for Foxp3+ regulatory T cells in K-Ras-driven lung tumorigenesis. PLoS One. 2009;4(3):e5061.
10. Haxhinasto S, Mathis D, Benoist C. The AKT-mTOR axis regulates de novo differentiation of CD4+Foxp3+ cells. J Exp Med. 2008;205(3):565–74.
11. Sauer S, Bruno L, Hertweck A, Finlay D, Leleu M, Spivakov M, et al. T cell receptor signaling controls Foxp3 expression via PI3K, Akt, and mTOR. Proc Natl Acad Sci U S A. 2008;105(22):7797–802.
12. de Miguel M, Calvo E. Clinical Challenges of Immune Checkpoint Inhibitors. Cancer Cell. 2020;38(3):326–33.
13. Kubli SP, Berger T, Araujo DV, Siu LL, Mak TW. Beyond immune checkpoint blockade: emerging immunological strategies. Nat Rev Drug Discov. 2021;20(12):899–919.
14. Ali K, Soond DR, Pineiro R, Hagemann T, Pearce W, Lim EL, et al. Inactivation of PI(3)K p110delta breaks regulatory T-cell-mediated immune tolerance to cancer. Nature. 2014;510(7505):407–11.
15. Brown KK, Toker A. The phosphoinositide 3-kinase pathway and therapy resistance in cancer. F1000Prime Rep. 2015;7:13.
16. De Henau O, Rausch M, Winkler D, Campesato LF, Liu C, Cymerman DH, et al. Overcoming resistance to checkpoint blockade therapy by targeting PI3Kgamma in myeloid cells. Nature. 2016;539(7629):443–7.
17. Gyori D, Chessa T, Hawkins PT, Stephens LR. Class (I) Phosphoinositide 3-Kinases in the Tumor Microenvironment. Cancers (Basel). 2017;9(3).
18. O'Donnell JS, Massi D, Teng MWL, Mandala M. PI3K-AKT-mTOR inhibition in cancer immunotherapy, redux. Semin Cancer Biol. 2018;48:91–103.
19. Budi EH, Muthusamy BP, Derynck R. The insulin response integrates increased TGF-beta signaling through Akt-induced enhancement of cell surface delivery of TGF-beta receptors. Sci Signal. 2015;8(396):ra96.

20. Nandan D, Camargo de Oliveira C, Moeenrezakhanlou A, Lopez M, Silverman JM, Subek J, et al. Myeloid Cell IL-10 Production in Response to Leishmania Involves Inactivation of Glycogen Synthase Kinase-3β Downstream of Phosphatidylinositol-3 Kinase. The Journal of Immunology. 2012;188(1):367–78.
21. Wu L, Derynck R. Essential role of TGF-beta signaling in glucose-induced cell hypertrophy. Dev Cell. 2009;17(1):35–48.
22. Abu-Eid R, Samara RN, Ozbun L, Abdalla MY, Berzofsky JA, Friedman KM, et al. Selective inhibition of regulatory T cells by targeting the PI3K-Akt pathway. Cancer Immunol Res. 2014;2(11):1080–9.
23. Vergadi E, Ieronymaki E, Lyroni K, Vaporidi K, Tsatsanis C. Akt Signaling Pathway in Macrophage Activation and M1/M2 Polarization. The Journal of Immunology. 2017;198(3):1006–14.
24. Peng W, Chen JQ, Liu C, Malu S, Creasy C, Tetzlaff MT, et al. Loss of PTEN Promotes Resistance to T Cell-Mediated Immunotherapy. Cancer Discov. 2016;6(2):202–16.
25. Lastwika KJ, Wilson W, 3rd, Li QK, Norris J, Xu H, Ghazarian SR, et al. Control of PD-L1 Expression by Oncogenic Activation of the AKT-mTOR Pathway in Non-Small Cell Lung Cancer. Cancer Res. 2016;76(2):227–38.
26. Yan C, Yang J, Saleh N, Chen SC, Ayers GD, Abramson VG, et al. Inhibition of the PI3K/mTOR Pathway in Breast Cancer to Enhance Response to Immune Checkpoint Inhibitors in Breast Cancer. Int J Mol Sci. 2021;22(10).
27. Isoyama S, Mori S, Sugiyama D, Kojima Y, Tada Y, Shitara K, et al. Cancer immunotherapy with PI3K and PD-1 dual-blockade via optimal modulation of T cell activation signal. J Immunother Cancer. 2021;9(8).
28. Zhang Y, Xu X, Yang K, Wang S, Zhang T, Hui F, et al. The efficacy and safety of PI3K and AKT inhibitors for patients with cancer: A systematic review and network meta-analysis. European Journal of Pharmacology. 2024;983:176952.
29. Saura C, Roda D, Rosello S, Oliveira M, Macarulla T, Perez-Fidalgo JA, et al. A First-in-Human Phase I Study of the ATP-Competitive AKT Inhibitor Ipatasertib Demonstrates Robust and Safe Targeting of AKT in Patients with Solid Tumors. Cancer Discov. 2017;7(1):102–13.
30. Mateo J, Ganji G, Lemech C, Burris HA, Han SW, Swales K, et al. A First-Time-in-Human Study of GSK2636771, a Phosphoinositide 3 Kinase Beta-Selective Inhibitor, in Patients with Advanced Solid Tumors. Clin Cancer Res. 2017;23(19):5981–92.
31. Seymour L, Bogaerts J, Perrone A, Ford R, Schwartz LH, Mandrekar S, et al. iRECIST: guidelines for response criteria for use in trials testing immunotherapeutics. Lancet Oncol. 2017;18(3):e143–e52.
32. Okada H, Weller M, Huang R, Finocchiaro G, Gilbert MR, Wick W, et al. Immunotherapy response assessment in neuro-oncology: a report of the RANO working group. Lancet Oncol. 2015;16(15):e534–e42.
33. Minchom A, Yuan W, Crespo M, Gurel B, Figueiredo I, Wotherspoon A, et al. Molecular and immunological features of a prolonged exceptional responder with malignant pleural mesothelioma treated initially and rechallenged with pembrolizumab. J Immunother Cancer. 2020;8(1).
34. Rescigno P, Lorente D, Dolling D, Ferraldeschi R, Rodrigues DN, Riisnaes R, et al. Docetaxel Treatment in PTEN- and ERG-aberrant Metastatic Prostate Cancers. Eur Urol Oncol. 2018;1(1):71–7.

35. Reid AH, Attard G, Brewer D, Miranda S, Riisnaes R, Clark J, et al. Novel, gross chromosomal alterations involving PTEN cooperate with allelic loss in prostate cancer. Mod Pathol. 2012;25(6):902–10.
36. Ferraldeschi R, Nava Rodrigues D, Riisnaes R, Miranda S, Figueiredo I, Rescigno P, et al. PTEN protein loss and clinical outcome from castration-resistant prostate cancer treated with abiraterone acetate. Eur Urol. 2015;67(4):795–802.
37. Thommen DS, Koelzer VH, Herzig P, Roller A, Trefny M, Dimeloe S, et al. A transcriptionally and functionally distinct PD-1(+) CD8(+) T cell pool with predictive potential in non-small-cell lung cancer treated with PD-1 blockade. Nat Med. 2018;24(7):994–1004.
38. Li H, van der Leun AM, Yofe I, Lubling Y, Gelbard-Solodkin D, van Akkooi ACJ, et al. Dysfunctional CD8 T Cells Form a Proliferative, Dynamically Regulated Compartment within Human Melanoma. Cell. 2019;176(4):775–89 e18.

FIGURE LEGENDS

Figure 1. Trial schema and patient disposition.
A. Patients with advanced solid tumors including relapsed GBM with limited treatment options were eligible. For Cohort A1, patients with advanced solid tumors were treated in two dose escalation cohorts receiving 200mg or 400mg oral Ipatasertib daily, for a two-week run-in course prior to commencing combination therapy with 1200 mg Atezolizumab intravenously three-weekly (Q3W). All patients in Cohort A1 consented to serial mandatory biopsies before and following ipatasertib monotherapy. Biopsies following one cycle of combination therapy were optional. Cohort A2 enrolled patients with relapsed GBM potentially suitable for re-resection and received at least two weeks of ipatasertib monotherapy prior to proceeding to surgery. Combination therapy with atezolizumab commenced following recovery from surgery. Disease assessment scans were performed every 3 cycles/9 weeks (Q9W). (Trial schema and patient disposition by Tiu, C. - stock.adobe.com/685673562)

B. Consort diagram showing the number of participants screened, enrolled, treated and analysed for exploratory translational endpoints are shown for Cohort A1, A2 and B3. Cohort A2 enrolled patients with potential resectable GBM, requiring three patients with evaluable tissue past resection. Over-recruitment was needed to ensure the minimum number of evaluable patients was met.

Figure 2. **Safety and tolerability data**. Volcano plots for **A.** Solid tumor Cohort A1 and **B.** GBM Cohorts A2 and B3, listing adverse presented as treatment-emergent AE (TEAEs) and treatment related AEs (TRAEs) by grade (NCI CTCAE, version 4.3)**.** See **Supp. Table 4** for safety data overview.

Figure 3. Antitumor activity of ipatasertib and atezolizumab in patients with relapsed GBM.

A. Panel describing clinical history of patient ICE101019. Serial MRI scans show gadolinium enhanced T1-weighted images (a1, b1 and c1) and apparent diffusion coefficient (ADC) maps (a2, b2 and c2) at the level of the midbrain. Viable tumor is delineated in red [Volume of interest (VOI) 2]; viable tumor with any additional abnormal, non-viable tissue (i.e. edema) is delineated in dashed green (VOI 3). The first follow-up MRI shows increased enhancement with gadolinium (b1) with marked increase in non-viable tissue (green delineation) in keeping with pseudo-progression (b2). Histological analysis of re-resection sample (January 2020) on H&E staining showed only inflammatory cells (e1) with gliosis (e2) without evidence of tumor confirming pathologic CR. This is in contrast to baseline H&E from initial surgery (d1, d2)

showing highly abnormal palisading cells with mitosis, consistent with glioblastoma. Post-resection, patient resumed IMP in February 2020 until August 2021 when MRI showed recurrence of gadolinium-enhanced tumor (c1) but with low ADC (c2) suggestive of true disease progression. (Patient ICE101019 clinical history by Tiu, C. - stock.adobe.com/685673562; stock.adobe.com/681274877)

B. Panel describing clinical history of patient ICE101106. Immediate post-operative MRI scans (a) showed residual disease (red arrow) in the posterior cavity margin after re-resection due to progression on second-line lomustine. Histological analysis of surgical sample confirmed recurrent GBM (not shown). Baseline scans (b) showed progression of residual disease (red arrows) on the left temporal lobe. First assessment after 2 cycles of treatment (c) showed SD but with noted increase in size and contrast enhancement of target lesion (blue arrow). Second reassessment after 4 cycles (d) showed reduction of left temporal disease (gold arrow) and reabsorption of brain oedema. Images (e) and (f) are from a slightly higher level of brain. Reassessment scans after 16 cycles (e) showed maintained PR with only non-specific subtle enhancement around the left temporal surgical cavity. Reassessment scans after 22 cycles (f) showed progressive disease with new small enhancing nodules (pink arrow) on the left temporal bone flap involving the meninges and brain surface. (Patient ICE101106 clinical history by Tiu, C. - stock.adobe.com/685673562; stock.adobe.com/681274877)

C. Waterfall plot demonstrating clinical activity in patients with relapsed GBM patients treated at 400mg dose level across cohorts A2 and B3 with evaluable baseline and at least one post-baseline assessment as per iRANO. Out of total n=17, only 16 patients are plotted. Baseline sum of diameters by RANO for ICE101038 was 0 hence the change is undefined.

D. Swimmer plot depicting, overall survival (OS), time on trial and best response of all GBM patients enrolled on study (n=24) as of cut-off date 21st March 2024. Patients who did not complete at least one cycle of treatment and were not evaluable for efficacy assessment are indicated in with a triangle. OS12 refers to OS at 12 months. Exceptional responders included patients who achieved pathological complete response (ICE101019), partial response (ICE101101), and patient with clinically stable disease for >12 months (ICE101045).

Figure 4

A. Ipatasertib depletes regulatory T cells regardless of somatic PI3KCA mutation status. Following the ipatasertib run-in period in Cohort A1, mIF of the tumor microenvironment showed a decrease in intratumoral and stromal CD4+FOXP3+ Tregs across all patients regardless of PI3KCA pathway mutation status. CD8+ T cell tumoral infiltration after ipatasertib-atezolizumab combination was increased in two responders (arrow). Graphs show median ± range; * indicates statistical significance with p-value <0.05, using two-tailed paired t-test. Sample size and statistical calculations are summarized in **Supp. Table 3**.

B. mIF of serial biopsies (baseline, post-ipatasertib run-in and post-combination ipatasertib-atezolizumab) from an example responder patient (ICE101013) with PIK3CA wildtype ER+ breast cancer. A marked reduction of regulatory CD4+FOXP3+ Tregs was seen following the two-week run-in with ipatasertib; and a significant increase in intratumoral CD8+ T cells following one cycle of ipatasertib-atezolizumab, suggesting a switch from a desert phenotype to an inflamed phenotype. Companion CT images at the same timepoints demonstrate a marked reduction in metastatic lung disease (orange arrows).

C. Marked increase in intratumoral CD8+ T cells was seen in two patients who had clinical benefit (PR or prolonged SD) following combination ipatasertib-atezolizumab (C2D1-baseline).

D. Two patients from A2 GBM cohort (ICE101016 and 101038) had tumor resected after the ipatasertib run-in period, while a third patient (ICE101019) had resection after 5 cycles of combination ipatasertib-atezolizumab. Further clinical history is described in (**Figure 3A**). (Cohort A2 window of opportunity by Tiu, C. - stock.adobe.com/685673562)

E. Changes in T cell counts in tumor samples from the two GBM patients who proceeded to re-resection following the ipatasertib run in. Similar to the solid tumor patients, both had reduction of CD4+FOXP3+ Tregs compared to archival diagnostic samples. One patient with a large increase [+73%, $\log_2$ fold change (FC)= 0.8] in effector CD8+ T cells had prolonged clinical benefit (ICE101016), while the other patient with minor change in effector CD8+ T cell numbers (+10%, $\log_2$FC=0.1) had progressive disease as the best response (ICE101038).

F-G. H&E and corresponding mIF images of patient ICE101016, demonstrating reduction in CD4+FOXP3+ regulatory T cells and increase in effector CD8+ T cells.

H-I. mIF images of resected samples from the exceptional responder (ICE101019) showing high levels of CD8+ effector T cells (50 cells/mm^2) at baseline, which remained elevated after combination treatment (36 cells/mm^2) ($\log_2$FC=-0.5). There was a notable increase in CD4+FOXP3- helper T cells (<0.01 to 2.75 cells/mm^2; $\log_2$FC=8.1).

J. There was increase in Th/Treg ratios in all paired tumor samples, with the highest change seen in exceptional responder (ICE101019) after combination therapy. Samples taken from ICE101016, who achieved SD after ipatasertib monotherapy, showed a greater Th/Treg shift compared to samples from ICE101038 who had PD.

Figure 5. Baseline CD8+ T cells and CD8A expression correlates with treatment response and overall survival in GBM patients.

A. mIF of archival samples demonstrated a significantly higher number of CD8+ effector T cells in patients who clinically benefitted [responders (R) or stable disease (SD) >6 months] on study compared to those who progressed (PD). Graphs indicate median ± 95% CI, with statistical significance of $p<0.05$ calculated by Mann-Whitney test (two-tailed).

B. Box plot showing CD8A gene expression in archival tumor samples was significantly higher in patients with clinical benefit (responders or SD >6 months) compared to non-responders (PD).

C. Kaplan-Meier survival curves for low, medium, and high CD8A expression groups; p-values calculated by log-rank test.

D. Heatmap of select Hallmark gene sets, CD8A cell signatures and exhaustion signatures in archival tumor of GBM patients(37, 38). Patients are arranged from high to low CD8A expression.

TABLES

Table 1. Patient baseline characteristics of those enrolled onto cohort A1 (solid tumor) and cohort A2 and B3 (relapsed GBM)

	Solid Tumors Cohort A1 (*n*=18)	**GBM** Cohort A2 (*n=12*) and Cohort B3 (*n=13*)
Age, median (range) years	49.6 (34.7 – 65.1)	56 (25.2 – 76.1)
Sex		
Female	15 (83.3%)	7 (28.0%)
Male	3 (16.7%)	18 (72.0%)
Race, n (%)		
White	15 (83%)	23 (92.0%)
Asian	2 (11.1%)	0 (0.0%)
Others	1 (5.6%)	2 (8.0%)
ECOG		
0	6 (33.3%)	2 (8.0%)
1	12 (66.7%)	23 (92.0%)
Tumor types, n (%)		
Glioblastoma		25 (100.0%)
IDH wildtype		23 (88%)
IDH mutant		2(12%)
Breast	11 (61.1%)	
Cervical	1 (5.6%)	
Prostate	1 (5.6%)	
Others*	5 (27.8%)	
Number of prior lines of therapy, median (range)	5 (1-11)	1.5 (0-4)
MGMT methylation status (A2 and B3 only) **Unmethylated** **Methylated** **Unknown**		13 (52%) 11 (44%) 1 (4%)
Median Time from Chemorradiation GBM IDH wildtype	Not applicable	11 (1-32) months
Aberration of PI3K-AKT pathway, n (%)* **Yes** **No**	11 (61%) 7 (29%)	Non-Applicable

***More information in Supplementary Table 1.**

ACKNOWLEDGEMENTS

The authors gratefully acknowledge that this research was a collaborative effort made possible through support from F. Hoffmann-La Roche Ltd for the imCORE Network. We also thank the Clinical Trials and Statistics Unit (CTSU) at The Institute of Cancer Research for statistical input, including the contributions of Xiaoran Lai, Guillermo Villacampa and Ben Jenkins. We also thank the contribution of Paul Johns, histopathologist at St. George's University Hospital. We also acknowledge infrastructural funding from the Experimental Cancer Medicine Centre (ECMCQQR-2022/100011); the National Institute of Health Sciences (NIHR) Biomedical Research Centre (BRC-NIHR-203314), to participating Centres; South London Clinical Research Network and Royal Marsden Cancer Charity. The authors from the Institute of Cancer Research acknowledge funding from the Cancer Research UK Convergence Science Centre grant (CTRQQR-2021\100009).
The views expressed are those of the authors and not necessarily those of the NIHR or the Department of Health and Social Care.

AUTHOR CONTRIBUTIONS

[JL, MA and IV] conceptualized and designed the clinical trial.
[CT, WY, DS, NW, MS, AB, LW, AC, TJ, AM, LB, NT, PB, PR, MR, AP, AS, UB, AM and JDB] were responsible for patient recruitment, clinical data collection, and patient management at their respective sites.
[XH, TP, MP, CY, CT, MB and MR] performed statistical analyses and interpreted the clinical and biomarker data.
[MC, AF, RR, BG, IF, DB, WY, RM, KS, IV and SD] led the correlative laboratory studies and biomarker assays.
[AZ, RD, AT and BB] managed regulatory submissions, ethics approval, and trial coordination.
[CT, DS and **JL]** wrote the manuscript with input from all authors.

Figure 1. Ice-CAP Phase 1b study design

A

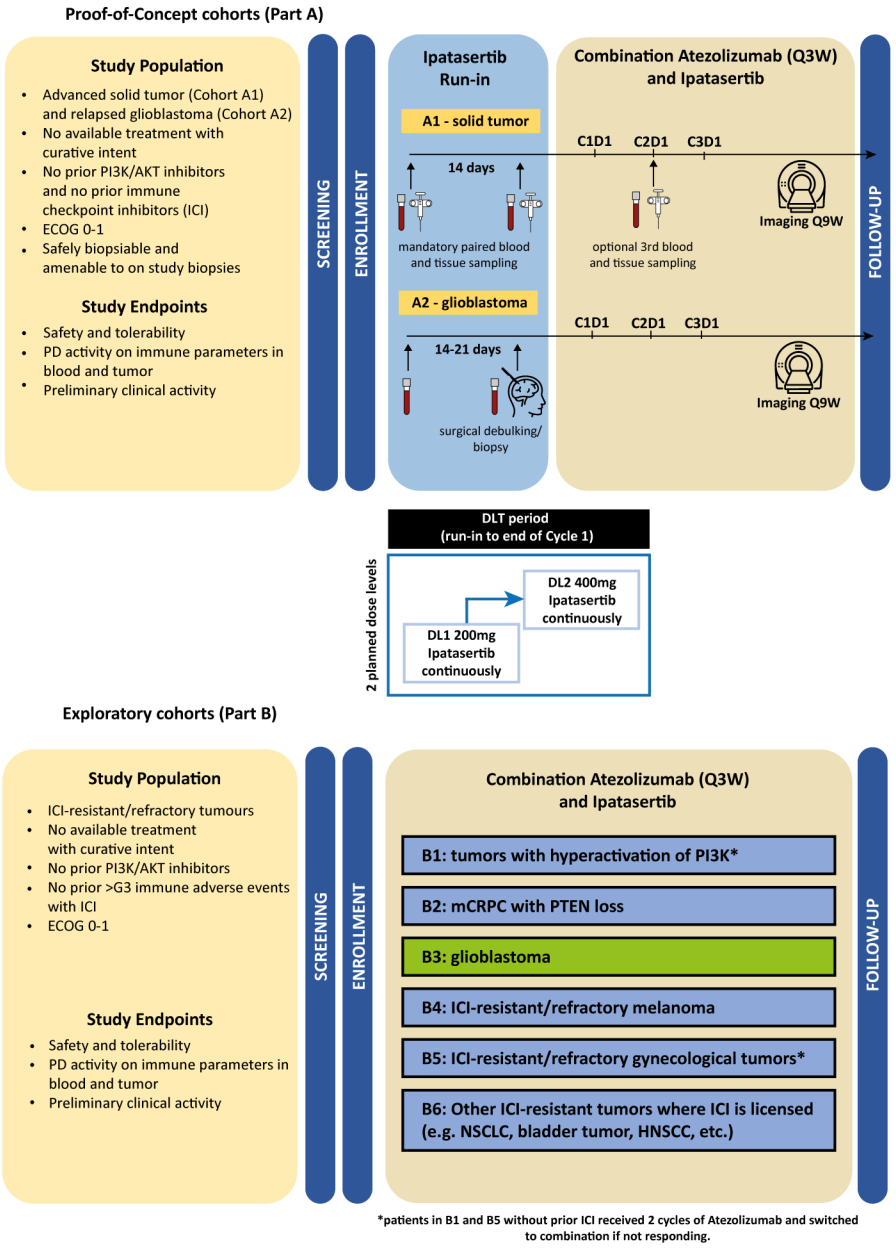

B

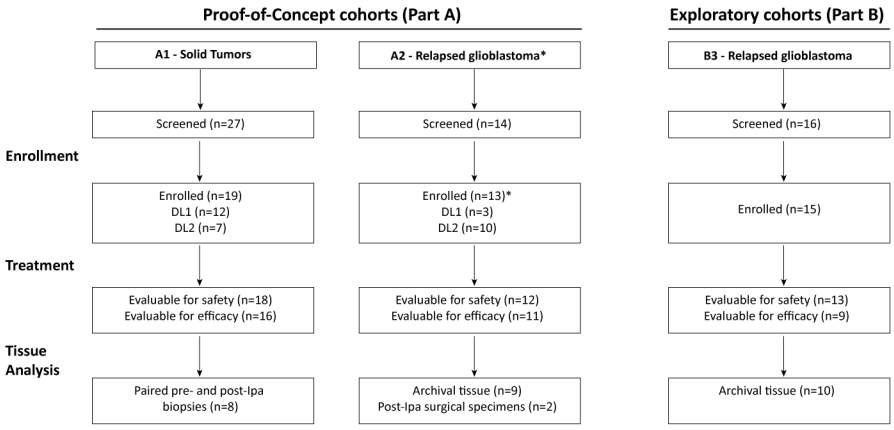

*Cohort A2 enrolled patients with potential resectable glioblastoma, requiring three patients with evaluable tissue past resection. Over recruitment was needed to ensure the minimum number of evaluable patients was met.

Figure 2. Volcano plots of all adverse events (AE) versus most common (incidence rate >15%) treatment-related adverse events (TRAE)

A Solid tumor cohort (A1)

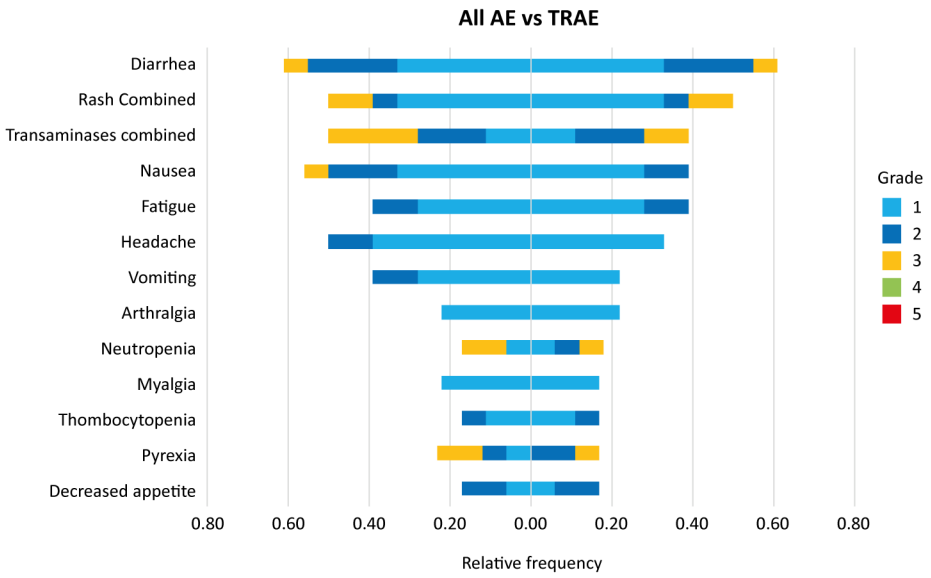

B Glioblastoma cohorts (A2 and B3)

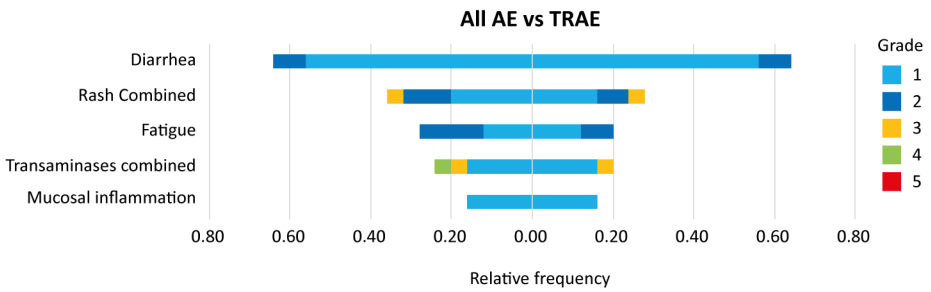

Figure 3

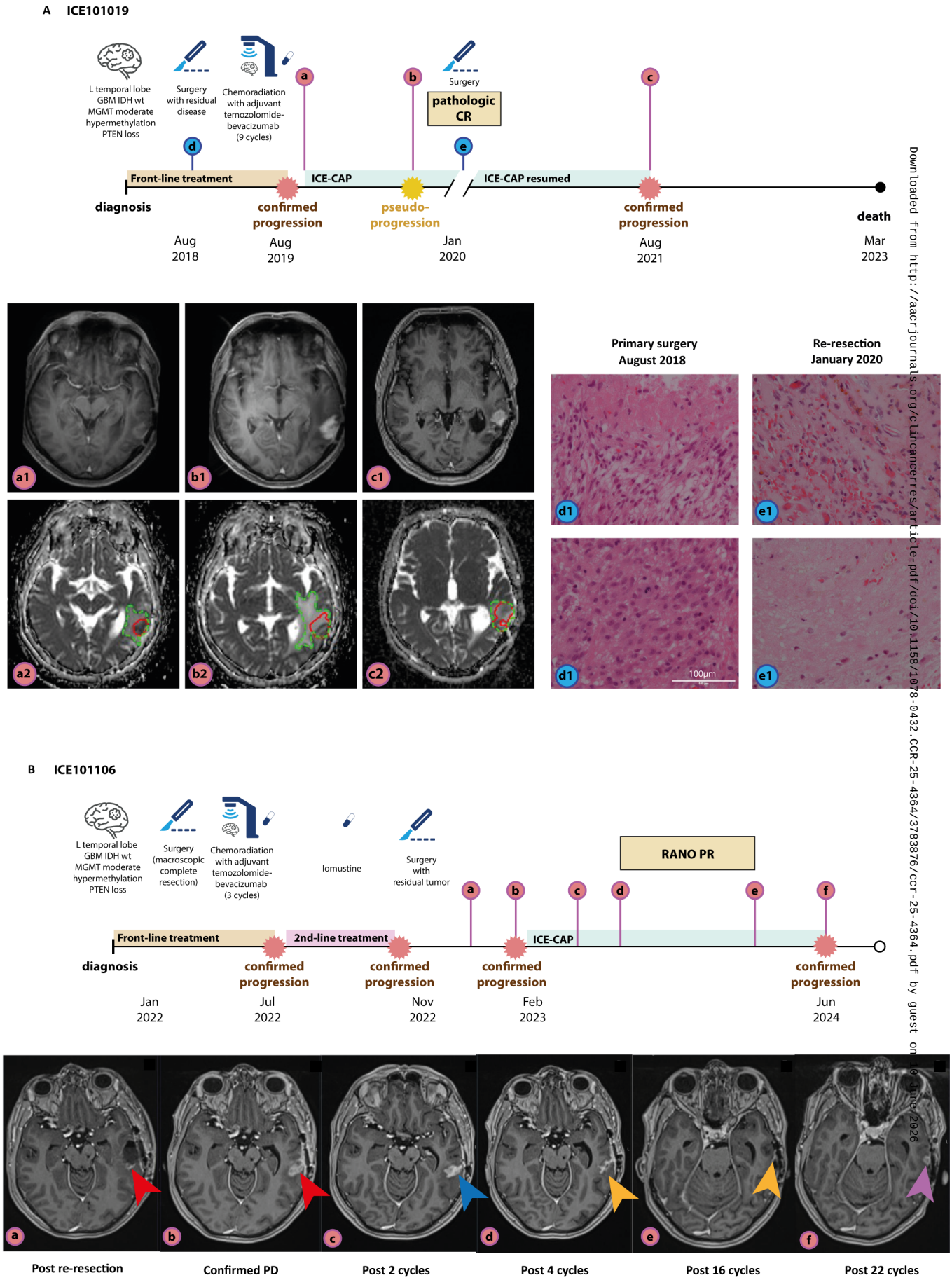

Figure 4.

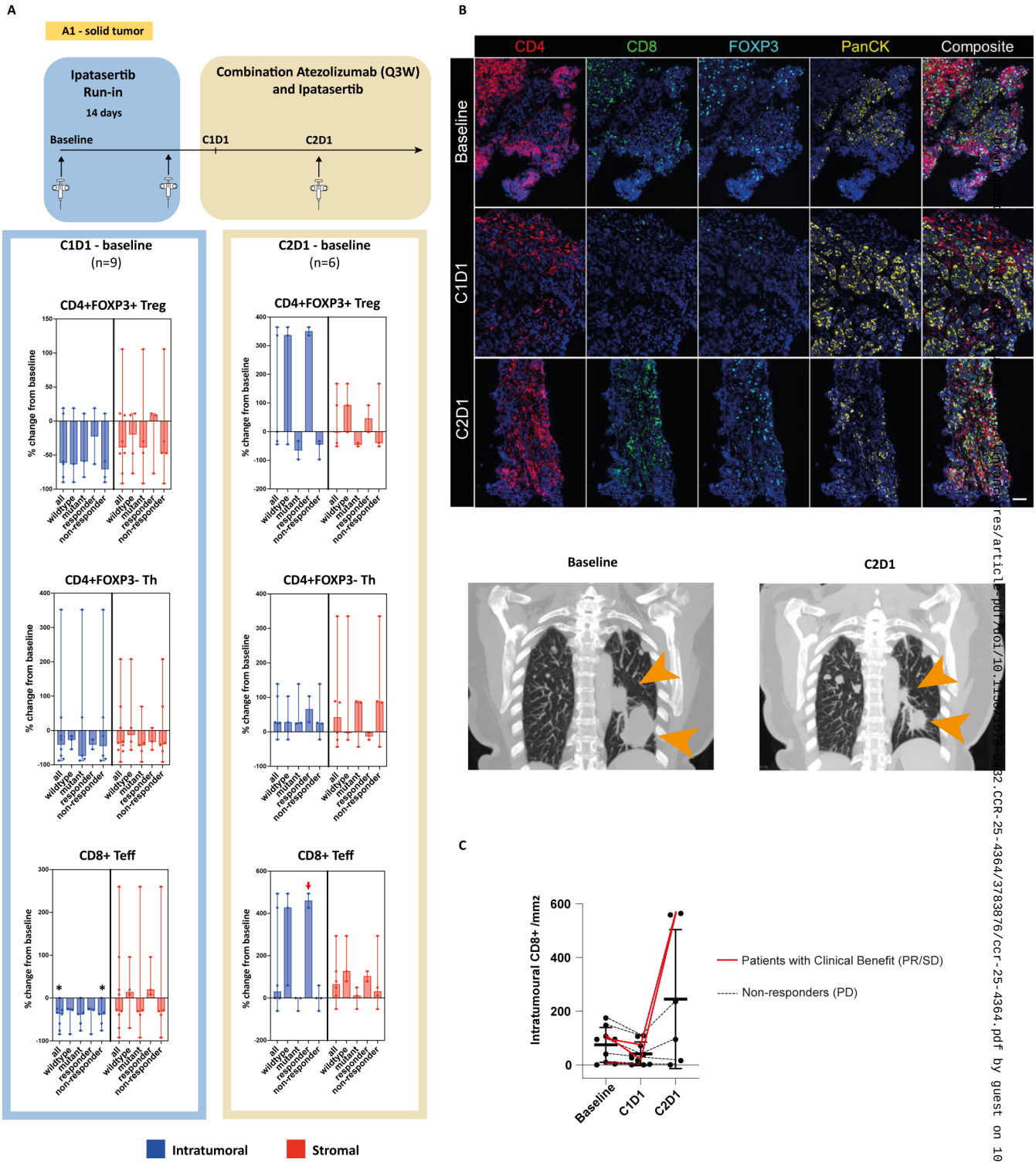

Figure 4

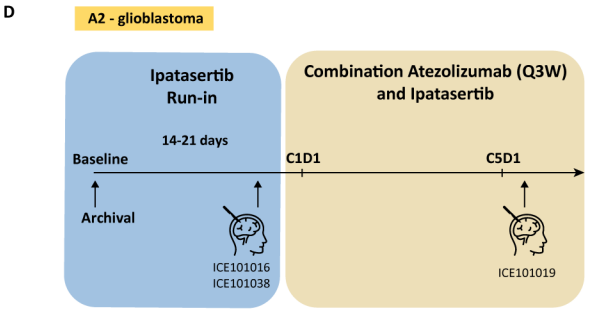

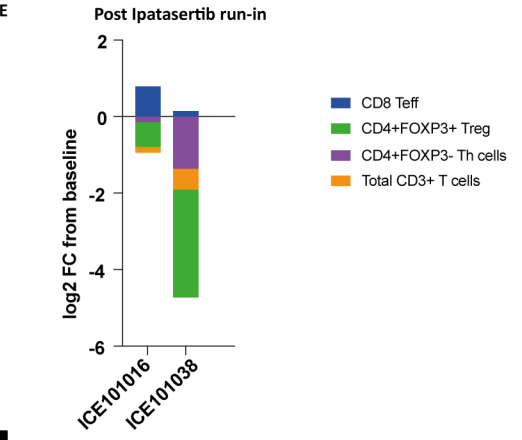

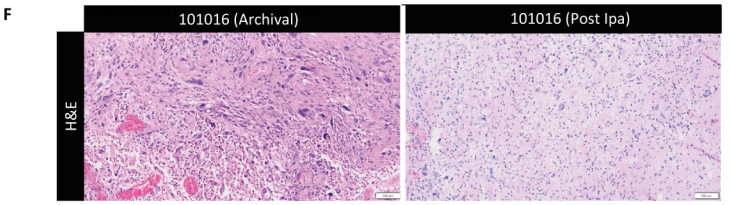

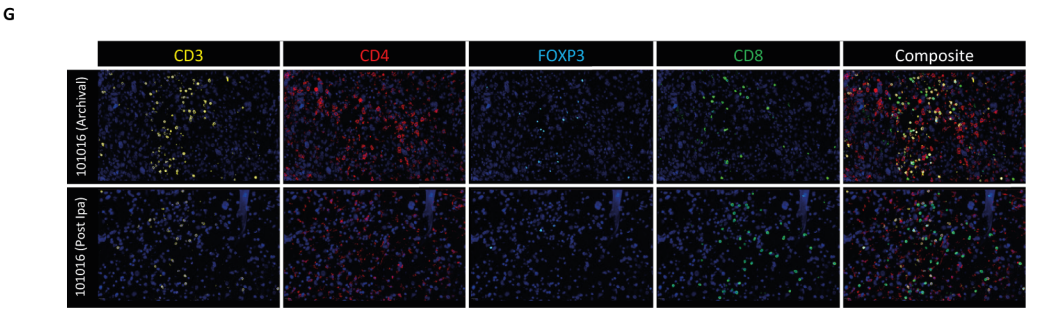

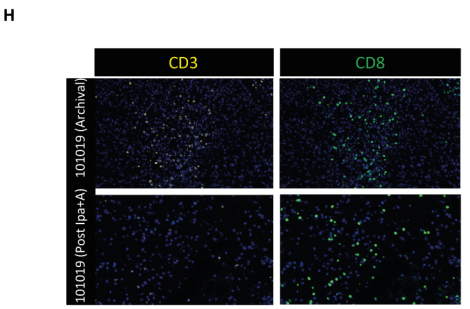

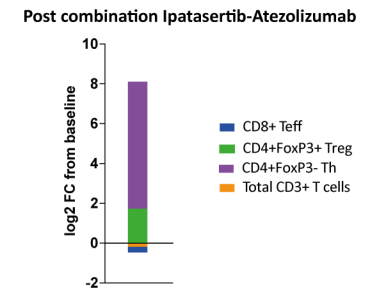

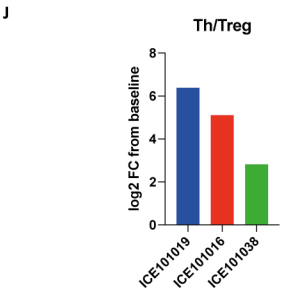

Patient ID	PTEN status	Best Response
ICE101019	loss	pCR
ICE101016	intact	SD
ICE101038	loss	PD

Figure 5. Baseline CD8+ T cells and CD8A expression correlates with treatment response and overall survival in GBM patients